Salidroside attenuates myocardial ischemia-reperfusion-induced oxidative stress and ferroptosis by promoting USP11-mediated deubiquitination of PRDX2

ZHI-CONG QIU[1,2*], JIAN-NAN LI[1,2*], YI-ZHOU LI[1,2*], ZI-MING WU[1,2], XU-DONG LUO[1,2], RUI-YUAN ZENG[1,2], SONG-QING LAI[1,2], SHI-TAO ZHAO[1,2] and LI WAN[1,2]

[1]Department of Cardiovascular Surgery, The First Affiliated Hospital of Nanchang University, Jiangxi Medical College, Nanchang University, Nanchang, Jiangxi 330006, P.R. China; [2]Institute of Cardiovascular Surgical Diseases, The First Affiliated Hospital of Nanchang University, Jiangxi Medical College, Nanchang University, Nanchang, Jiangxi 330006, P.R. China

Received April 16, 2026; Accepted September 8, 2026

DOI: 10.3892/ijmm.2026.6000

Abstract. Myocardial ischemia/reperfusion (I/R) injury is closely associated with excessive oxidative stress and ferroptosis. Salidroside (Sal), a major active component of *Rhodiola*, has demonstrated cardioprotective properties, yet its precise mechanisms in regulating ferroptosis remain unclear. The present study investigated whether Sal attenuates myocardial I/R injury by modulating ubiquitin-specific protease 11 (USP11)-mediated deubiquitination and stabilization of peroxiredoxin 2 (PRDX2). An *in vitro* H9c2 anoxia/reoxygenation (A/R) model and an *in vivo* rat I/R model were established. Sal significantly improved the viability of A/R-injured H9c2 cells and reduced reactive oxygen species accumulation, ferrous iron overload and lipid peroxidation. Mechanistically, Sal upregulated the expression levels of USP11, glutathione peroxidase 4 and PRDX2 while suppressing prostaglandin-endoperoxide synthase 2; notably, these effects were attenuated by USP11 silencing. Molecular docking and cellular thermal shift assay analyses suggested that USP11 may represent a potential molecular target involved in Sal-mediated cardioprotection, thereby increasing its thermal stability and strengthening the USP11-PRDX2 interaction. This may facilitate the USP11-mediated stabilization of PRDX2, prolonging its half-life and preserving cellular redox homeostasis. *In vivo* experiments further demonstrated that Sal pretreatment markedly reduced myocardial infarct size and improved cardiac contractile function, which was associated with the concurrent upregulation of the USP11-PRDX2 axis. Collectively, these findings indicate that Sal confers robust cardioprotection against I/R injury by engaging USP11 and promoting the stabilization of PRDX2, thereby suppressing oxidative stress and ferroptosis. USP11 represents a promising therapeutic target for mitigating myocardial I/R injury.

Introduction

Myocardial ischemia/reperfusion (I/R) injury represents a notable clinical challenge in cardiovascular disease, commonly observed in conditions such as acute myocardial infarction and cardiac surgery (1,2). Following the restoration of blood flow to ischemic myocardial tissue, accumulated metabolites, oxygen-derived free radicals and other harmful substances generated during the ischemic phase trigger the production of damaging agents, such as reactive oxygen species (ROS), reactive nitrogen species and lipid peroxidation products (3,4). This initiates a cascade of complex pathophysiological responses, including excessive oxidative stress, mitochondrial dysfunction, inflammatory responses and cardiomyocyte death, which severely compromise cardiac function and may even prove fatal (5). Consequently, investigating the underlying mechanisms of myocardial I/R injury and developing effective preventive and therapeutic strategies are major research priorities in cardiovascular science (6).

In previous years, ferroptosis, an iron-dependent form of regulated cell death driven by excessive lipid peroxide accumulation, has gained increasing attention for its role in myocardial I/R injury (7,8). Under physiological conditions, cells maintain iron homeostasis through sophisticated regulatory mechanisms, ensuring iron participation in essential

Correspondence to: Dr Li Wan or Dr Shi-Tao Zhao, Department of Cardiovascular Surgery, The First Affiliated Hospital of Nanchang University, Jiangxi Medical College, Nanchang University, 17 Yongwai Zheng Road, Nanchang, Jiangxi 330006, P.R. China
E-mail: ndyfy02131@ncu.edu.cn
E-mail: ndyfy07996@ncu.edu.cn

*Contributed equally

Abbreviations: I/R, ischemia/reperfusion; A/R, anoxia/reoxygenation; Sal, salidroside; USP11, ubiquitin-specific protease 11; PRDX2, peroxiredoxin 2; ROS, reactive oxygen species; GPX4, glutathione peroxidase 4; PTGS2, prostaglandin-endoperoxide synthase 2; LAD, left anterior descending; Fer-1, ferrostatin-1; CETSA, cellular thermal shift assay; Co-IP, co-immunoprecipitation

Key words: salidroside, myocardial ischemia/reperfusion injury, USP11, PRDX2, oxidative stress, ferroptosis

biological processes including oxygen transport, electron transfer and DNA synthesis (9,10). However, during myocardial I/R injury, intracellular iron homeostasis becomes disrupted, leading to notable iron accumulation (11). The excess iron ions (primarily Fe^{2+}) catalyze generation of ROS, particularly the oxidative hydroxyl radical, through the Fenton reaction (12). These ROS molecules subsequently attack polyunsaturated fatty acids in cell membranes, initiating severe lipid peroxidation. When lipid peroxide production exceeds cellular clearance capacity, such as when the function of key antioxidant defense systems including glutathione peroxidase 4 (GPX4) is compromised, membrane integrity becomes destroyed, leading to irreversible cell death (13,14). A study has demonstrated that the ferroptosis-specific inhibitor ferrostatin-1 (Fer-1) effectively mitigates myocardial I/R injury, providing interventional evidence for the role of ferroptosis in this pathological process (15).

Oxidative stress constitutes a fundamental pathological event in myocardial I/R injury (16). When the myocardium experiences an I/R insult, the balance between oxidative and antioxidant systems becomes disrupted, resulting in excessive ROS generation and/or impaired antioxidant capacity. During myocardial I/R, the increase in ROS primarily originates from mitochondrial dysfunction and NADPH oxidase activation (17). In the early reperfusion phase, the mitochondrial electron transport chain serves as a major ROS source (18). Concurrently, various I/R-related stimuli, including calcium overload, inflammatory cytokines and angiotensin II, activate NADPH oxidases located on cell membranes and mitochondria, directly catalyzing ROS production (19). Excessive ROS not only directly damage cellular components, inducing lipid peroxidation, protein inactivation and DNA damage, but also activate intricate intracellular signaling networks that amplify cellular injury (20). For instance, ROS can activate the inflammasome, promoting pro-inflammatory cytokine release and establishing a vicious cycle of damage (21).

A tight interplay exists between oxidative stress and ferroptosis (22). Oxidative stress disrupts intracellular iron metabolism, promoting free ferrous ion accumulation, while ROS-driven lipid peroxide accumulation represents a hallmark of ferroptosis. Thus, in myocardial I/R injury, oxidative stress and ferroptosis form a positive feedback loop through multiple molecular mechanisms, mutually promoting cardiomyocyte dysfunction and death (11).

Plants of the *Rhodiola* genus have a long history of use in traditional medicine. Salidroside (Sal), the primary active component of *Rhodiola*, has attracted considerable interest due to its diverse pharmacological properties, including antioxidant, anti-hypoxic, anti-fatigue and anti-inflammatory effects (23). In the cardiovascular system, Sal has been shown to ameliorate myocardial I/R injury, reduce infarct size and improve cardiac function (24); its antioxidant activity, potentially mediated through direct ROS scavenging and modulation of antioxidant enzymes such as superoxide dismutase (SOD), is considered a key mechanism underlying these protective effects (25). However, the impact of Sal on myocardial I/R-induced ferroptosis and its precise molecular mechanisms require further investigation.

Ubiquitin-specific protease 11 (USP11), a deubiquitinating enzyme family member, regulates substrate stability, activity and localization by removing ubiquitin molecules from target proteins (26). USP11 participates in various cellular processes including DNA damage repair and cell cycle progression (27). Emerging evidence suggests that USP11 may influence cellular oxidative stress responses by deubiquitinating and stabilizing sirtuin 3, thereby regulating oxidative stress-induced ferroptosis (28). However, its specific role in myocardial I/R injury remains unclear.

Peroxiredoxin 2 (PRDX2), a ubiquitously expressed antioxidant enzyme, serves roles in maintaining cellular redox homeostasis by efficiently scavenging ROS such as hydrogen peroxide and peroxides (29). Under oxidative stress conditions, PRDX2 function can be altered by post-translational modifications such as S-nitrosylation, which may affect its antioxidant activity and mitochondrial homeostasis, thereby influencing cell survival and function (30). The stability and activity of PRDX2 are modulated by various factors, with S-nitrosylation serving as a prominent regulatory mechanism (31). Nonetheless, the potential impact of ubiquitination on PRDX2 degradation and function necessitates further exploration.

The present study aimed to investigate the effects of Sal on ferroptosis and oxidative stress markers, along with its regulatory role on USP11 and PRDX2 expression and ubiquitination, using an *in vitro* H9c2 cell model of A/R injury and an *in vivo* Sprague-Dawley (SD) rat model of myocardial I/R injury. The findings from the present study will help elucidate the molecular mechanisms through which Sal alleviates myocardial I/R injury.

Materials and methods

Reagents and antibodies. Sal (purity ≥98%) was purchased from Beijing Solarbio Science & Technology Co., Ltd. Fer-1 (cat. no. HY-100579) and erastin (cat. no. HY-15763) were obtained from MedChemExpress. Sal and Fer-1 were dissolved in DMSO. The final concentration of DMSO in the cellular culture medium was <0.1% (v/v) for all experiments to preclude any vehicle-induced cytotoxicity. Primary antibodies against USP11 (cat. no. R22861; ZenBio; Chengdu Zhengneng Biotechnology Co., Ltd.), ubiquitin (cat. no. R382766; ZenBio; Chengdu Zhengneng Biotechnology Co., Ltd.), PRDX2 (cat. no. R27157; ZenBio; Chengdu Zhengneng Biotechnology Co., Ltd.), GPX4 (cat. no. 30388-1-AP; Proteintech Group, Inc.), prostaglandin-endoperoxide synthase 2 (PTGS2; cat. no. AF7003; Affinity Biosciences) and β-actin (cat. no. TA-09; Beijing Zhongshan Jinqiao Biotechnology Co., Ltd.) were used. Horseradish peroxidase (HRP)-conjugated goat anti-rabbit (cat. no. 511203; ZenBio; Chengdu Zhengneng Biotechnology Co., Ltd.) and goat anti-mouse (cat. no. 511103; ZenBio; Chengdu Zhengneng Biotechnology Co., Ltd.) antibodies served as secondary antibodies.

Animals. A total of 18 male SD rats (8 weeks old; weighing 250±20 g) were obtained from Hubei Tianqin Biotechnology Group Co., Ltd. Rats were housed under standard laboratory conditions at a temperature of 22-24˚C and relative humidity of 40-60%, with a 12-h light/dark cycle. All rats had free access to food and water throughout the experimental period and were randomized into experimental groups using a random number table. Outcome assessments were conducted in a blinded manner. All animal experiments were approved

by the Ethics Committee of the First Affiliated Hospital of Nanchang University (Nanchang, China; approval no. CDYFY-IACUC-2025092003) and conducted in accordance with the National Institutes of Health guidelines.

In vivo experiments

Animal experiments. The myocardial I/R model was established as previously described (32). A total of 18 rats were used in the study, with 6 rats in each group. Rats were randomly assigned to three groups: The sham group underwent thoracotomy without left anterior descending (LAD) ligation; the I/R group received 4 weeks of daily normal saline gavage before I/R surgery; and the I/R + Sal group received 4 weeks of daily Sal (50 mg/kg/day) gavage before I/R surgery. This dosage was selected based on a previous study demonstrating its robust cardioprotective efficacy against myocardial I/R injury without inducing systemic toxicity (33). Rats were monitored daily for general health and behavior throughout the experimental period, including activity, food and water intake, body weight, posture and signs of pain or distress. Animals were euthanized if they exhibited severe or persistent signs of distress, including marked reductions in activity or food/water intake, severe respiratory distress, inability to ambulate or maintain normal posture or other signs of severe pain that could not be alleviated. No animals met the predefined humane endpoint criteria during the present study. The total experimental period was 4 weeks of daily gavage followed by myocardial I/R surgery and 2 h of reperfusion. Briefly, rats were anesthetized with isoflurane (induction at 3%, maintenance at 1.5%) and mechanically ventilated, followed by hair removal and a left thoracotomy at the fourth intercostal space to expose the heart. The LAD coronary artery was ligated with a 7-0 silk suture for 30 min of ischemia, after which the ligature was released to allow 2 h of reperfusion. The chest was closed in layers with a 4-0 silk suture after evacuating residual air from the pleural cavity. At the end of the experiment, echocardiographic assessment was performed, followed by blood collection from all rats while they remained under anesthesia. According to the American Veterinary Medical Association Guidelines for the Euthanasia of Animals (34), rats were euthanized by a deep anesthetic overdose using 5% isoflurane, and death was confirmed by cessation of respiration and heartbeat. No rats died during surgery or the experimental period; no animals were found dead and no animals were excluded from the final analysis. All 18 rats were euthanized at the end of the experiment.

Echocardiographic measurements. Under isoflurane anesthesia, left ventricular function was assessed using M-mode echocardiography [V6 lead, 23 MHz linear transducer; VINNO Technology (Suzhou) Co., Ltd.] to measure left ventricular fractional shortening (LVFS) and left ventricular ejection fraction (LVEF).

Measurement of lactate dehydrogenase (LDH) and creatine kinase isoenzyme (CK-MB) levels. After echocardiographic measurement and while under isoflurane anesthesia, ~2 ml blood was collected from the abdominal aorta. The rats were then immediately euthanized. Blood samples were stored at 4˚C overnight and then centrifuged at 12,000 x g for 15 min at 4˚C to obtain serum. LDH and CK-MB levels were determined using corresponding assay kits (LDH, cat. no. A020-2-2; CK-MB, cat. no. H197-1-1; Nanjing Jiancheng Bioengineering Institute) as per the manufacturer's protocol.

Triphenyl tetrazolium chloride (TTC) staining. Following euthanasia, the hearts were immediately excised, washed with PBS and frozen at -20˚C for 30 min. Each heart was sliced into 2 mm sections, followed by incubation in 2% TTC solution (cat. no. C0652; Beyotime Biotechnology) at 37˚C in the dark for 30 min. Digital images of the heart slices were obtained and analyzed using ImageJ software (version 1.8.0; National Institutes of Health). To quantify myocardial infarct size, the infarcted area and the total ventricular slice area were measured manually in a blinded manner. The infarct size was calculated as the percentage of the infarcted area relative to the total ventricular slice area (used as the denominator).

H&E staining. Myocardial tissue samples used for H&E staining were collected separately from those used for TTC staining and were not subjected to the freezing procedure. Following the respective treatments, the tissues were fixed in 4% paraformaldehyde at room temperature for 24 h. The fixed tissues were then dehydrated, embedded in paraffin and sectioned at a thickness of 5 μm. According to the manufacturer's instructions (cat. no. G1076; Wuhan Servicebio Technology Co., Ltd.), sections were stained with hematoxylin at room temperature for 10 min, followed by eosin staining at room temperature for 2 min. Stained sections were observed and imaged at x400 magnification using an optical microscope (LX73; Olympus Corporation).

In vitro experiments

Cell culture. H9c2 cells were purchased from the Cell Bank/Stem Cell Bank of the Chinese Academy of Sciences. The cells were cultured in Dulbecco's Modified Eagle Medium (DMEM; Beijing Solarbio Science & Technology Co., Ltd.; cat. no. 12100) supplemented with 10% fetal bovine serum (FBS; cat. no. ZQ0500; Shanghai Zhongqiao Xinzhou Biotechnology Co., Ltd.) and 1% penicillin-streptomycin and maintained at 37˚C in a humidified atmosphere containing 5% CO_2.

Anoxia/reoxygenation (A/R) injury model. In accordance with a previous study, an H9c2 cell A/R injury model was established to simulate *in vivo* I/R injury (35). Briefly, cells were incubated in an anoxic buffer containing 1.0 mM $CaCl_2$, 20.0 mM HEPES, 10.0 mM KCl, 1.2 mM $MgSO_4$, 98.5 mM NaCl, 0.9 mM NaH_2PO_4, 6.0 mM $NaHCO_3$ and 40.0 mM sodium lactate (pH 6.8) for 4 h at 37˚C under anoxia conditions (95% N_2 and 5% CO_2). Subsequently, the medium was replaced with a reoxygenation solution composed of 1.0 mM $CaCl_2$, 5.5 mM glucose, 20.0 mM HEPES, 5.0 mM KCl, 1.2 mM $MgSO_4$, 129.5 mM NaCl, 0.9 mM NaH_2PO_4 and 20.0 mM $NaHCO_3$ (pH 7.4), and cells were further incubated for 4 h at 37˚C in a sealed chamber equilibrated with 95% O_2 and 5% CO_2.

Cell transfection. To investigate the role of USP11 in myocardial I/R injury, genetic manipulations were performed in H9c2 cells to knock down or overexpress USP11. For USP11 knockdown, small interfering (si) RNA (si-USP11) and its negative control (si-NC) (Shanghai Focus Bioscience Co., Ltd.; Table SI) were transfected into H9c2 cells at a final concentration of 50 nM using jetOPTIMUS transfection reagent (cat. no. 101000006; Polyplus-transfection SA) according

to the manufacturer's instructions. The cells were incubated at 37˚C in a humidified atmosphere containing 5% CO_2, and subsequent experiments were performed after 48 h of transfection. For USP11 overexpression, the USP11 empty vector (USP11-EV; pCMV-3xFLAG-Neo) and USP11 overexpression plasmid [USP11-OE; pCMV-Usp11(rat)-3xFLAG-Neo] were constructed using the same pCMV-3xFLAG-Neo backbone and obtained from Wuhan MiaoLing Biotech Science Co., Ltd. The plasmids were transfected into H9c2 cells using 4-6 μg of plasmid DNA per transfection with HighGene plus transfection reagent (cat. no. RM09014P; ABclonal Biotech Co., Ltd.) following the manufacturer's protocol. The cells were incubated at 37˚C in a humidified atmosphere containing 5% CO_2 for 6 h during transfection, after which the culture medium was replaced. Subsequent experiments were performed 48 h after transfection.

H9c2 cells treatment. All treatments were performed at 37˚C. The experimental design consisted of the following groups: i) Control group of H9c2 cells maintained under standard culture conditions; ii) A/R group of H9c2 cells subjected to A/R injury; iii) Sal concentration-dependent group of H9c2 cells pretreated with varying concentrations of Sal (1.25, 2.5, 5, 10, 20 and 40 μM) for 48 h; iv) Sal concentration-dependent + A/R group of H9c2 cells pretreated with Sal at concentrations of 1.25, 2.5, 5, 10, 20 and 40 μM for 48 h, followed by A/R injury; v) 10 μM Sal + A/R group of H9c2 cells pretreated with 10 μM Sal for 48 h prior to A/R injury; vi) Fer-1 + A/R group of H9c2 cells pretreated with 5 μM Fer-1 for 2 h prior to A/R injury; vii) erastin group of H9c2 cells pretreated with 10 μM erastin for 24 h prior to protein extraction (this group served strictly as a positive methodological control to validate the efficacy of the ferroptosis detection assays, rather than to model A/R injury); viii) 10 μM Sal + si-USP11 + A/R group of H9c2 cells transfected with si-USP11 and pretreated with 10 μM Sal for 48 h before A/R injury; and ix) USP11-OE + A/R group of H9c2 cells transfected with USP11-OE for 48 h prior to A/R injury.

Cell viability assay. Cell viability was assessed using the Cell Counting Kit-8 (CCK-8; cat. no. GK10001; GLPBIO Technology LLC) according to the manufacturer's instructions. H9c2 cells were seeded into 96-well plates and subjected to the indicated treatments. Subsequently, serum-free DMEM containing 10% CCK-8 solution was added. The cells were then incubated at 37˚C for 30 min and the optical density was measured at a wavelength of 450 nm.

Lipid peroxidation assay. Lipid peroxidation levels in H9c2 cells were evaluated by measuring 4-hydroxynonenal (4-HNE) and malondialdehyde (MDA) contents. MDA levels were quantified using an MDA assay kit (cat. no. S0131; Beyotime Biotechnology) and 4-HNE levels were determined using a 4-HNE assay kit (cat. no. JL46304; Jianglai Biotechnology Co., Ltd.), according to the manufacturers' instructions.

To further assess lipid peroxidation, a boron-dipyrromethene (BODIPY) 581/591 C11 lipid peroxidation assay kit (cat. no. S0043; Beyotime Biotechnology) was used according to the manufacturer's instructions. The BODIPY 581/591 C11 probe was diluted 1:1,000 to a final concentration of 2 μM and incubated with H9c2 cells at 37˚C in the dark for 20 min. After three washes with PBS, fluorescence images were captured using an optical microscope (LX73; Olympus Corporation) at x200 magnification. Red fluorescence indicates the non-oxidized form of the BODIPY 581/591 C11 probe, whereas green fluorescence indicates the oxidized form, reflecting increased lipid peroxidation.

Measurement of SOD, glutathione disulfide (GSSG) and glutathione (GSH) levels. After the designated treatments, cell lysates were collected from each group. SOD activity (cat. no. S0101S; Beyotime Biotechnology) and the levels of reduced GSH and oxidized GSSG (cat. no. S0053; Beyotime Biotechnology) were measured according to the manufacturer's instructions. The GSH/GSSG ratio was subsequently calculated.

Measurement of intracellular ROS. Intracellular ROS levels were measured using a ROS assay kit (cat. no. S0033S; Beyotime Biotechnology). The 2',7'-dichlorodihydrofluorescein diacetate probe was diluted to a final concentration of 10 μM and incubated with H9c2 cells at 37˚C in the dark for 20 min. Cells were then washed three times with PBS and fluorescence images were captured using fluorescence microscopy (LX73; Olympus Corporation) at x100 magnification.

Ferrous ion detection. Ferrous ion levels in H9c2 cells were assessed using a ferrous ion detection kit (cat. no. F374; Dojindo Molecular Technologies, Inc.). According to the manufacturer's instructions, the FerroOrange working solution was prepared and diluted with Hank's balanced salt solution to a final concentration of 1 μM. Cells were incubated with the 1 μM working solution at 37˚C in the dark for 30 min. Fluorescence images were subsequently acquired using an optical microscope (magnification, x200; LX73; Olympus Corporation).

Co-immunoprecipitation (Co-IP). Cells were lysed in RIPA buffer (cat. no. R0010; Beijing Solarbio Science & Technology Co., Ltd.) supplemented with protease and phosphatase inhibitors. Lysates were centrifuged at 12,000 x g for 15 min at 4˚C and total protein concentrations were determined using a BCA protein assay kit. To ensure equal total protein input across all experimental groups, equal amounts of total protein from each sample were adjusted to the same final volume and used for each IP reaction. Each reaction contained 600 μl of lysate and was incubated with 3 μl of anti-PRDX2 antibody at 4˚C with gentle rotation overnight. Protein A+G agarose beads (50 μl suspension; cat. no. P2055; Beyotime Biotechnology) were then added and the mixture was incubated for an additional 8 h at 4˚C with gentle rotation. The agarose beads were collected by centrifugation at 3,000 x g for 30 sec at room temperature, washed three times with PBST (0.1% Tween-20) and boiled directly in SDS-PAGE loading buffer. The immunoprecipitants were subsequently separated by 10% SDS-PAGE and analyzed using western blotting.

Western blotting. Following the respective treatments, cells were lysed in RIPA buffer containing 1% PMSF (cat. no. R0010; Beijing Solarbio Science & Technology Co., Ltd.). The lysates were collected and protein concentrations were determined using a BCA Protein Assay Kit (cat. no. GK10009; GLPBIO Technology LLC). Equal amounts of protein (30 μg) were separated by 10% SDS-PAGE and transferred onto PVDF membranes. The membranes were blocked with 5% non-fat milk for 2 h at room temperature, followed by incubation with primary antibodies at 4˚C overnight. The primary antibodies used were PTGS2, GPX4, USP11, PRDX2,

ubiquitin and β-actin (all at 1:1,000). After incubation with HRP-conjugated secondary antibodies (1:5,000) for 2 h at room temperature, protein bands were visualized using an Ultra-High Sensitivity ECL Kit (cat. no. GK10008; GLPBIO Technology LLC) and imaged with a FluorChem FC3 system (ProteinSimple). All immunoblot experiments were performed in at least three independent biological replicates. Target protein expression was normalized to the corresponding β-actin internal loading control. Band intensities were semi-quantified using ImageJ software (version 1.8.0; National Institutes of Health).

Cellular thermal shift assay (CETSA). Cell lysates were prepared as aforementioned and the supernatants were collected. Each lysate was divided into two equal portions and incubated with Sal (10 μM) or DMSO (0.1%) at room temperature for 30 min. The samples were then aliquoted into six equal fractions and heated at 50, 54, 58, 62, 66 or 70˚C for 3 min. Following heat treatment, samples were centrifuged at 12,000 x g for 15 min at 4˚C, and the resulting supernatants were collected, mixed with loading buffer, boiled and subsequently subjected to western blot analysis. As a control experiment to assess the thermal stability of USP11 at 50˚C, cell lysates were divided into equal portions and treated with Sal (10 μM) or DMSO (0.1%) at room temperature for 30 min, followed by heating at 34, 38, 42, 46 or 50˚C for 3 min. Samples were then processed for western blot analysis, and USP11 band intensities were quantified. Notably, a conventional loading control (such as β-actin) was not employed in this assay, as the majority of cellular proteins undergo unpredictable thermal denaturation across the applied temperature gradient. Instead, the reliability of the assay was ensured by strictly equalizing the starting protein concentration and dividing the lysates into equal aliquots prior to heat treatment, in accordance with established pioneering CETSA protocols (36-38). USP11 does not undergo significant thermal denaturation at 50˚C; therefore, for quantitative analysis the band intensity at 50˚C was defined as the intact baseline reference (100%) and the subsequent temperature points were normalized to this value to determine the thermal denaturation curves.

Cycloheximide (CHX) chase assay. H9c2 cells were transfected with si-USP11 and/or treated with Sal (10 μM), as indicated. Subsequently, cells were treated with CHX (10 μg/ml; cat. no. HY-12320; MedChemExpress) to inhibit *de novo* protein synthesis. Cells were collected at 0, 6, 12 and 24 h after CHX treatment, and total protein was extracted and analyzed by western blotting. The protein levels of USP11 and PRDX2 were determined, with β-actin used as the loading control. PRDX2 stability was assessed by comparing its relative protein abundance at each time point with that at 0 h.

Ubiquitination analysis. H9c2 cells were treated with Sal (10 μM) and/or transfected with si-USP11 according to the experimental design. MG132 (10 μM; cat. no. HY-13259; MedChemExpress) was added 4 h before protein collection to inhibit proteasomal degradation. Cell lysates were subjected to immunoprecipitation with an anti-PRDX2 antibody following the procedure described for the Co-IP assay. The resulting immunoprecipitants were subsequently analyzed by western blotting with an anti-ubiquitin antibody to assess PRDX2 ubiquitination.

Molecular docking. Molecular docking was performed using CB-Dock2 (http://clab.labshare.cn/cb-dock2/) (39,40). The three-dimensional structure of USP11 (PDB ID, 4MEM) was obtained from the Protein Data Bank (http://www.rcsb.org/) (41) and that of Sal (PubChem CID, 159278) was retrieved from the PubChem database (https://pubchem.ncbi.nlm.nih.gov/).

Statistical analysis. Statistical analyses were performed using GraphPad Prism (version 8.0.2; Dotmatics). The exact number of independent biological replicates for each individual experiment is specified in the corresponding figure legends. Data distribution was evaluated for normality using the Shapiro-Wilk test. Data are presented as the mean ± standard deviation. Differences between two groups were assessed using an unpaired Student's t-test. Comparisons among multiple groups were conducted using one-way ANOVA followed by Tukey's multiple comparison post hoc test. Exact P-values are provided in the figure legends and results text where possible. $P<0.05$ was considered to indicate a statistically significant difference.

Results

Sal pretreatment alleviates A/R injury in H9c2 cells. Fig. 1A shows the chemical structure of Sal. To evaluate the biosafety and optimal protective concentration of Sal, separate evaluations were performed under normoxic and A/R conditions. First, to assess potential baseline cytotoxicity, normal H9c2 cells were treated with increasing concentrations of Sal (0 to 40 μM) for 48 h under normoxic conditions. As demonstrated in Fig. 1B, cell viability remained unaffected across this entire concentration range, confirming that Sal exhibits no intrinsic cytotoxicity. Second, to determine cardioprotective efficacy, H9c2 cells were pretreated with the same concentration gradient of Sal for 48 h, after which the Sal-containing medium was replaced with specific anoxic and reoxygenation buffers to induce A/R injury. As demonstrated in Fig. 1C, A/R injury markedly reduced cell viability; however, this detrimental effect was attenuated by Sal pretreatment in a bell-shaped concentration-dependent manner, with the optimal protective effect observed at 10 μM. Therefore, a 48-h pretreatment with 10 μM Sal was selected for all subsequent mechanistic experiments.

Sal attenuates A/R-induced oxidative stress and ferroptosis in H9c2 cells. To determine whether Sal exerts cardioprotective effects by suppressing oxidative stress and ferroptosis, a systematic evaluation of key associated indicators was conducted. Considering that erastin can simultaneously induce oxidative stress and ferroptosis (42), erastin-treated cells were utilized as a positive control to validate the ferroptosis detection system. The results demonstrated that A/R injury produced ferroptotic marker alterations comparable to those induced by erastin; however, while this phenotypic similarity is supportive, the mechanistic involvement of ferroptosis in A/R injury was further corroborated by the protective effects of the specific inhibitor Fer-1. Western blot analysis demonstrated that A/R injury significantly upregulated the downstream ferroptosis-associated marker PTGS2 while

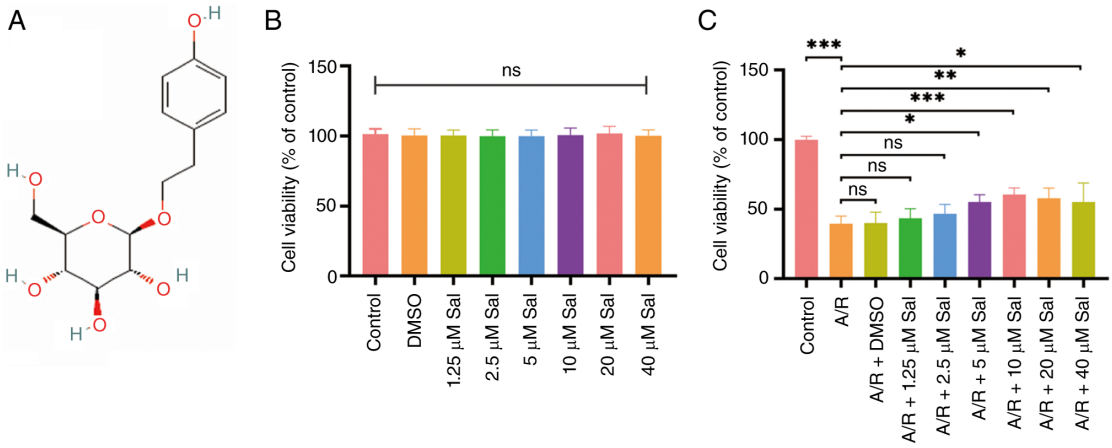

Figure 1. Sal pretreatment alleviates A/R injury in H9c2 cells. (A) Chemical structure of Sal. (B) H9c2 cells were treated with increasing concentrations of Sal (0 to 40 μM) for 48 h under normoxic conditions and cell viability was assessed using the CCK-8 assay (n=6). (C) H9c2 cells were pretreated with different concentrations of Sal (0 to 40 μM) for 48 h, followed by replacement with anoxic and reoxygenation buffers to induce A/R injury. Cell viability was measured using CCK-8 assay to determine the protective concentration range (n=6). Data are presented as mean ± SD, with *P<0.05, **P<0.01 and ***P<0.001 indicating statistical significance. ns, not significant; Sal, salidroside; A/R, anoxia/reoxygenation; CCK-8, Cell Counting Kit-8.

downregulating the ferroptosis-related protein GPX4 and the oxidative stress-related protein PRDX2. Pretreatment with Sal or the ferroptosis inhibitor Fer-1 (5 μM) attenuated these alterations in protein expression (Fig. 2A and B). Further analyses revealed that A/R injury markedly increased intracellular ROS, ferrous ion levels and lipid peroxidation, whereas pretreatment with Sal or Fer-1 significantly attenuated these elevations (Fig. 2C-E). Moreover, assessment of oxidative and antioxidative parameters demonstrated that MDA and 4-HNE levels were markedly elevated in the A/R group, accompanied by pronounced reductions in SOD activity and the GSH/GSSG ratio. Notably, treatment with Sal and Fer-1 effectively reversed these alterations, as evidenced by decreased levels of MDA and 4-HNE, along with increased SOD activity and GSH/GSSG ratio (Fig. 2F-I). Given the previously reported involvement of USP11 in oxidative stress-induced ferroptosis (28), USP11 expression was also examined to explore its potential involvement in A/R injury. Notably, compared with the control group, A/R injury resulted in a significant downregulation of USP11 expression in H9c2 cells, whereas pretreatment with Sal or Fer-1 partially restored USP11 expression (Fig. 2A and B). Collectively, these findings indicated that Sal may attenuate A/R-induced oxidative stress and protect cells against ferroptotic injury, although whether these effects are mediated via USP11 requires further investigation.

Sal mitigates A/R-induced oxidative stress and ferroptosis in H9c2 cells by enhancing USP11-mediated signaling. To determine whether Sal confers protection against A/R-induced oxidative stress and ferroptosis through USP11, a USP11-OE plasmid and a specific siRNA (si-USP11) were constructed, and their transfection efficiencies verified using western blotting (Fig. 3A and B). Subsequent experiments demonstrated that Sal pretreatment significantly increased the expression levels of USP11, GPX4 and PRDX2, while suppressing PTGS2 expression. However, silencing USP11 abolished these effects, as evidenced by increased PTGS2 levels and reduced USP11, GPX4 and PRDX2 expression (Fig. 3C and D). These findings indicated that Sal may alleviate A/R-induced oxidative stress and ferroptosis through the upregulation of USP11. Oxidative stress and ferroptosis-related cellular parameters were further evaluated. Sal markedly reduced A/R-induced ROS accumulation, ferrous iron overload and lipid peroxidation. USP11 knockdown notably weakened the inhibitory effects of Sal on ROS accumulation and lipid peroxidation, while partially attenuating its effect on ferrous iron accumulation (Fig. 3E-G). Biochemical analyses, including MDA, 4-HNE, SOD activity and the GSH/GSSG ratio, consistently supported the potential role of USP11 in mediating the antioxidative and anti-ferroptotic actions of Sal (Fig. 3H-K). Consistently, USP11 overexpression was associated with a coordinated attenuation of the A/R-induced oxidative stress and ferroptotic phenotype, including reduced PTGS2 expression, ROS accumulation, ferrous iron overload and lipid peroxidation, MDA and 4-HNE levels, accompanied by increased GPX4 and PRDX2 expression, SOD activity and GSH/GSSG ratio (Fig. 3C-K). Taken together, these results demonstrated that Sal may suppress A/R-induced oxidative stress and ferroptosis in H9c2 cells through the upregulation of USP11.

Sal binds to USP11 and enhances the USP11-PRDX2 interaction in H9c2 cells. Based on the aforementioned findings, PRDX2 was selected as a potential downstream target of USP11 since its expression changed in parallel with USP11 and was responsive to USP11 knockdown and overexpression. In addition, PRDX2 is an antioxidant protein whose stability may be influenced by ubiquitination, providing a mechanistic basis for investigating whether it is regulated by the deubiquitinase, USP11. Therefore, it was hypothesized that Sal may directly interact with USP11 and thereby modulate its association with PRDX2. To test this, molecular docking, Co-IP and CETSA assays were performed. Molecular docking using CB-Dock2 revealed that Sal fits into several potential binding cavities of USP11, with the C5 pocket showing the highest affinity (Vina score: -7.5; Fig. 4A). Consistently, Co-IP analysis demonstrated that A/R injury markedly attenuated the USP11-PRDX2 interaction, whereas Sal pretreatment effectively restored their binding (Fig. 4B). Furthermore, CETSA demonstrated that Sal

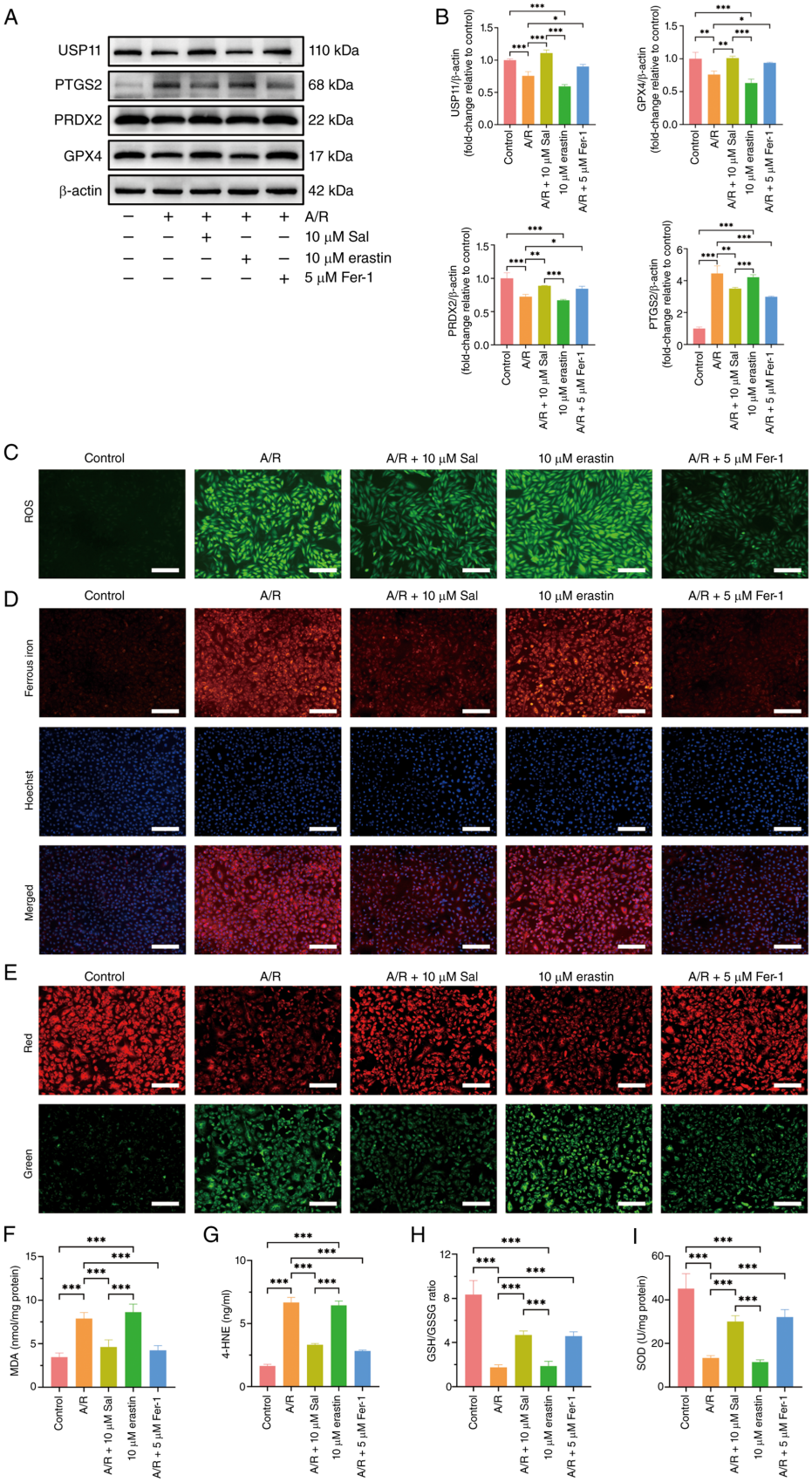

Figure 2. Sal attenuates A/R-induced oxidative stress and ferroptosis in H9c2 cells. (A) Western blot analysis of PTGS2, GPX4, PRDX2 and USP11 proteins in different groups of H9c2 cells (n=3). (B) Relative expression analysis of PTGS2, GPX4, PRDX2 and USP11 (n=3). (C) Intracellular ROS levels detected using 2',7'-dichlorodihydrofluorescein diacetate fluorescence staining (magnification, x100; scale bar, 800 μm; n=3). (D) Intracellular ferrous iron levels measured using FerroOrange probe (magnification, x200; scale bar, 400 μm; n=3). (E) Lipid peroxidation assessed using boron-dipyrromethene 581/591 C11 fluorescence staining (magnification, x200; scale bar, 400 μm; n=3). Biochemical quantification of (F) MDA, (G) 4-HNE, (H) GSH/GSSG ratio and (I) SOD activity (n=6). Data are presented as mean ± SD, with *P<0.05, **P<0.01 and ***P<0.001 indicating statistical significance. Sal, salidroside; Fer-1, ferrostatin-1; A/R, anoxia/reoxygenation; PTGS2, prostaglandin-endoperoxide synthase 2; GPX4, glutathione peroxidase 4; PRDX2, peroxiredoxin 2; USP11, ubiquitin-specific protease 11; ROS, reactive oxygen species; MDA, malondialdehyde; 4-HNE, 4-hydroxynonenal; GSSG, glutathione disulfide; GSH, glutathione; SOD, superoxide dismutase.

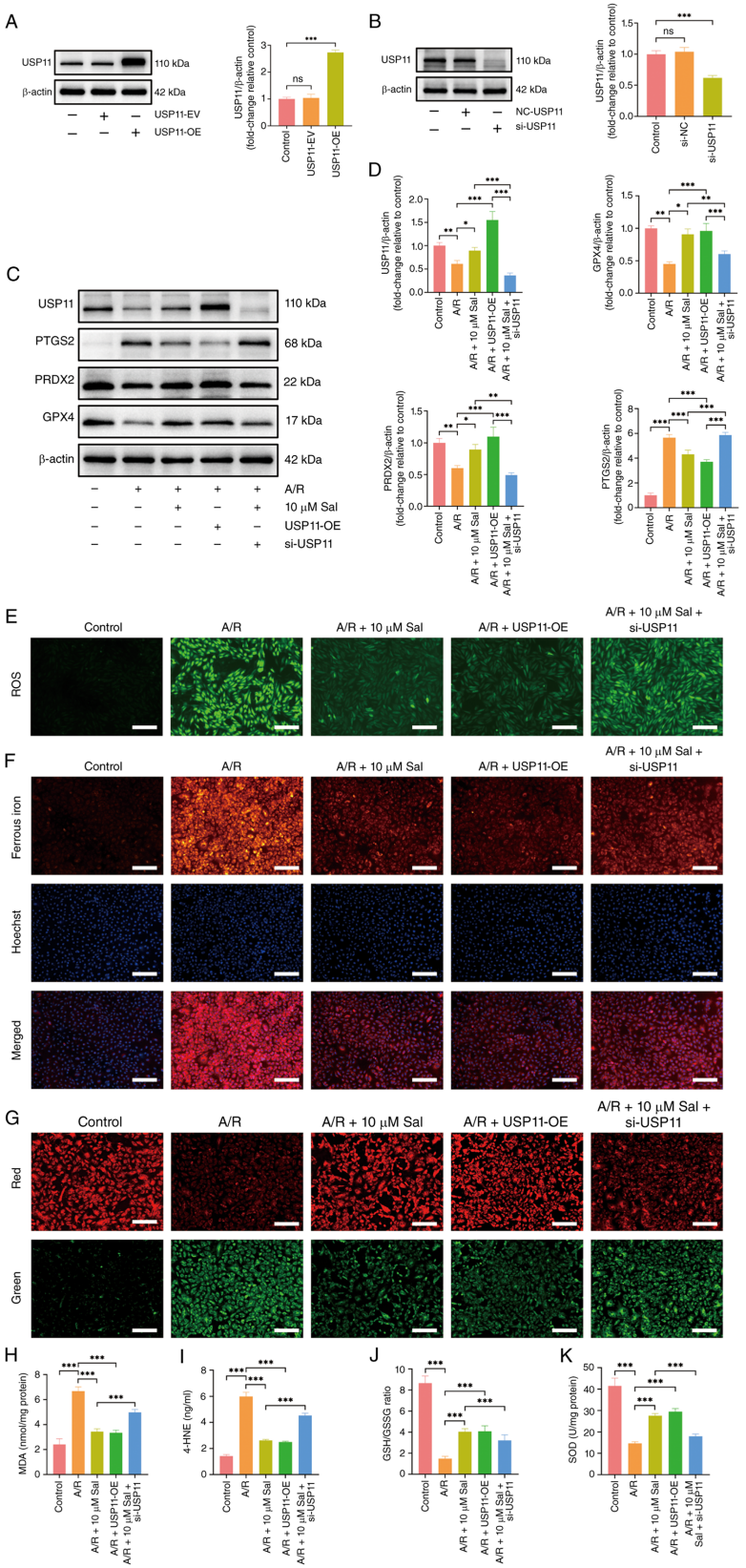

Figure 3. Sal mitigates A/R-induced oxidative stress and ferroptosis in H9c2 cells by enhancing USP11-mediated signaling. Validation of USP11 (A) silencing (si-USP11) and (B) overexpression (USP11-OE) efficiency in H9c2 cells via western blotting (n=3). (C) Western blot analysis of PTGS2, GPX4, PRDX2 and USP11 proteins in different groups of H9c2 cells (n=3). (D) Relative expression analysis of PTGS2, GPX4, PRDX2 and USP11 (n=3). (E) Intracellular ROS levels detected using 2',7'-dichlorodihydrofluorescein diacetate fluorescence staining (magnification, x100; scale bar, 800 μm; n=3). (F) Intracellular ferrous iron levels measured using FerroOrange probe (magnification, x200; scale bar, 400 μm; n=3). (G) Lipid peroxidation assessed using boron-dipyrromethene 581/591 C11 fluorescence staining (magnification, x200; scale bar, 400 μm; n=3). Biochemical quantification of (H) MDA, (I) 4-HNE, (J) GSH/GSSG ratio and (K) SOD activity (n=6). Data are presented as mean ± SD, with *P<0.05, **P<0.01 and ***P<0.001 indicating statistical significance. ns, not significant; Sal, salidroside; A/R, anoxia/reoxygenation; PTGS2, prostaglandin-endoperoxide synthase 2; GPX4, glutathione peroxidase 4; PRDX2, peroxiredoxin 2; USP11, ubiquitin-specific protease 11; ROS, reactive oxygen species; MDA, malondialdehyde; 4-HNE, 4-hydroxynonenal; GSSG, glutathione disulfide; GSH, glutathione; SOD, superoxide dismutase; si, small interfering; OE, overexpression; EV, empty vector.

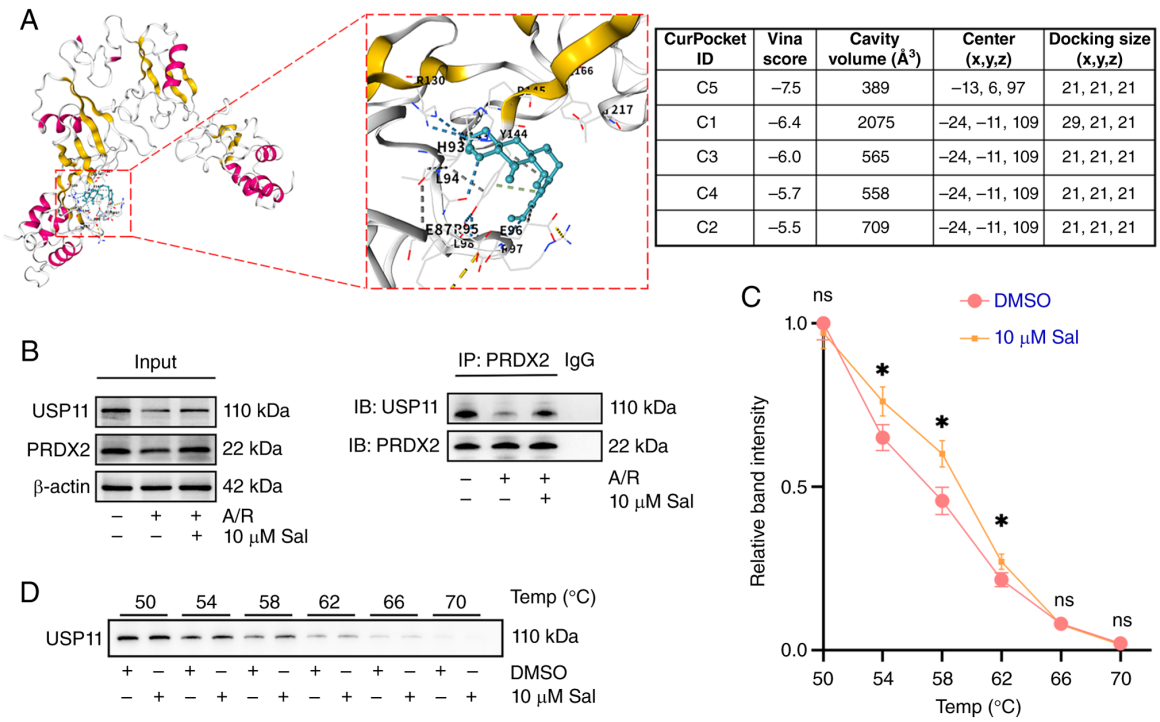

CurPocket ID	Vina score	Cavity volume (Å^3)	Center (x,y,z)	Docking size (x,y,z)
C5	−7.5	389	−13, 6, 97	21, 21, 21
C1	−6.4	2075	−24, −11, 109	29, 21, 21
C3	−6.0	565	−24, −11, 109	21, 21, 21
C4	−5.7	558	−24, −11, 109	21, 21, 21
C2	−5.5	709	−24, −11, 109	21, 21, 21

Figure 4. Sal binds to USP11 and enhances the USP11-PRDX2 interaction in H9c2 cells. (A) Molecular docking simulation using CB-Dock2, predicting the binding mode of Sal in the C5 pocket of the USP11 protein. (B) Co-IP assay performed using H9c2 cells to assess the physical interaction between USP11 and PRDX2 under A/R and Sal-treatment conditions (n=3). (C) Quantification of the relative USP11 band intensity following CETSA in cell lysates treated with DMSO or Sal (10 μM) across a temperature gradient of 50-70˚C (n=3). (D) Representative CETSA western blot showing the thermal stability of USP11 in cell lysates treated with DMSO or Sal (10 μM) across the same temperature gradient. Data are presented as mean ± SD, with *P<0.05 indicating statistical significance. ns, not significant; Sal, salidroside; USP11, ubiquitin-specific protease 11; PRDX2, peroxiredoxin 2; Co-IP, co-immunoprecipitation; A/R, anoxia/reoxygenation; CETSA, cellular thermal shift assay.

increased the thermal stability of USP11, supporting an interaction between Sal and USP11 (Fig. 4C and D). Preliminary thermal evaluations confirmed that USP11 does not undergo significant thermal denaturation or precipitation up to 50˚C and Sal treatment alone did not alter baseline USP11 solubility within this lower temperature range (Fig. S1). These results suggest that Sal may exert cardioprotective effects through modulation of USP11-associated signaling and strengthening its interaction with PRDX2.

Sal enhances USP11-mediated deubiquitination and stabilization of PRDX2. The aforementioned findings demonstrated an interaction between USP11 and PRDX2 and showed that PRDX2 expression was responsive to changes in USP11 levels. These observations prompted further investigation into whether USP11 regulates PRDX2 stability through deubiquitination and whether Sal modulates this process. To determine whether Sal stabilizes PRDX2 in a USP11-dependent manner, CHX chase assays were performed. Silencing USP11 markedly shortened the half-life of PRDX2, whereas Sal treatment effectively attenuated the accelerated degradation caused by USP11 depletion (Fig. 5A and B). Consistently, ubiquitination analyses revealed that Sal reduced PRDX2 ubiquitination, while USP11 knockdown exerted the opposite effect and significantly increased PRDX2 ubiquitination (Fig. 5C and D). Together, these results demonstrate that Sal may stabilize PRDX2 by enhancing USP11-mediated deubiquitination, thereby contributing to its protective effects against A/R injury.

Sal pretreatment protects the myocardium against I/R injury. To evaluate the protective effect of Sal against myocardial I/R injury *in vivo*, a rat model of LAD coronary artery ligation was established. Compared with the sham-operated group, the serum levels of the myocardial injury markers CK-MB and LDH were markedly elevated following I/R injury (Fig. 6A and B), and the infarct area increased markedly (Figs. 6F and S2). Echocardiography further demonstrated severe cardiac dysfunction in the I/R group, evidenced by pronounced reductions in LVEF and LVFS (Fig. 6C-E). Sal pretreatment effectively attenuated these alterations, thereby mitigating myocardial damage and functional decline. Morphological assessment revealed that I/R injury induced myofibrillar disarray, cardiomyocyte swelling and interstitial edema with inflammatory infiltration, as shown by H&E staining, whereas these pathological abnormalities were markedly ameliorated by Sal pretreatment (Fig. 6G). Analysis of oxidative stress- and ferroptosis-related proteins demonstrated increased PTGS2 expression and decreased USP11, GPX4 and PRDX2 expression after I/R injury; Sal pretreatment attenuated these molecular changes (Fig. 6H-L). Collectively, these findings indicate that Sal pretreatment may confer cardioprotection by modulating the expression levels of USP11 and other related proteins, thereby mitigating I/R-induced oxidative injury and ferroptosis.

Discussion

In the present study, an *in vitro* A/R model using H9c2 cells was combined with an *in vivo* rat model of myocardial I/R

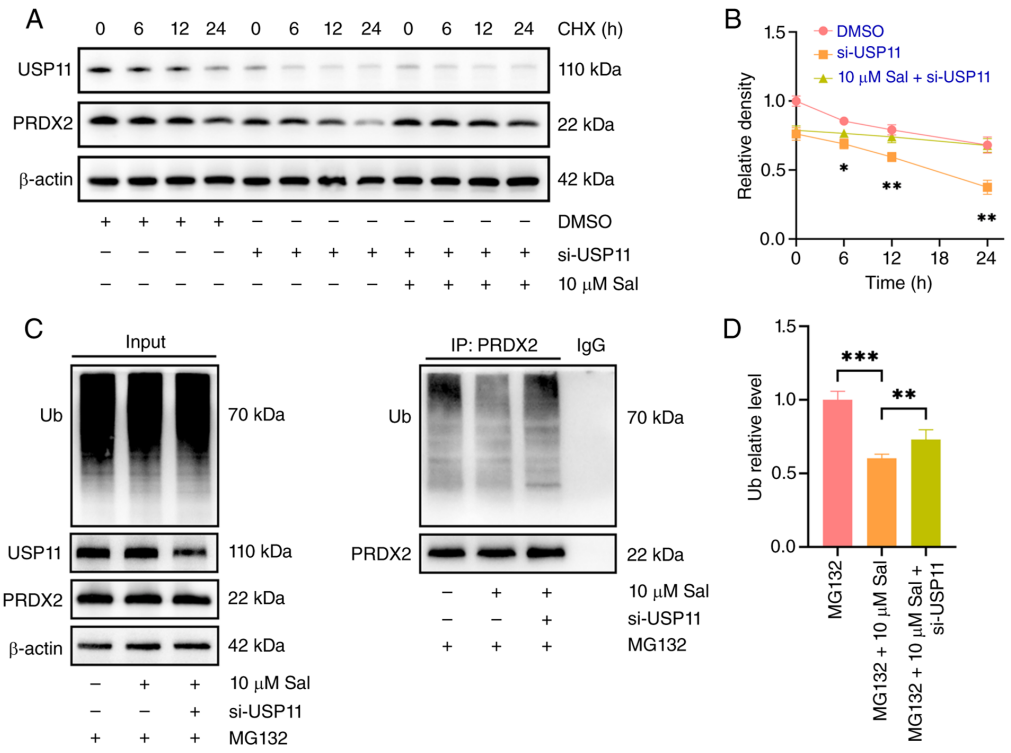

Figure 5. Sal enhances USP11-mediated deubiquitination and stabilization of PRDX2. (A) Representative western blot analysis of USP11 and PRDX2 in H9c2 cells treated with CHX (10 μg/ml) for 0, 6, 12 and 24 h in the presence or absence of Sal and si-USP11 (n=3). (B) Semi-quantification of PRDX2 protein levels during the CHX chase assay (n=3; si-USP11 vs. 10 μM Sal + si-USP11). (C) Representative western blot analysis of PRDX2 ubiquitination in H9c2 cells treated with Sal and/or si-USP11 in the presence of MG132. The ubiquitination smear represents the extent of PRDX2 polyubiquitination (n=3). (D) Semi-quantitative analysis of the ubiquitination levels of PRDX2 (n=3). Data are presented as mean ± SD, with *P<0.05, **P<0.01 and ***P<0.001 indicating statistical significance. Sal, salidroside; USP11, ubiquitin-specific protease 11; PRDX2, peroxiredoxin 2; CHX, cycloheximide; si, small interfering; Ub, ubiquitin.

injury to systematically investigate the cardioprotective effects of Sal and its underlying molecular mechanisms. The present results demonstrated that Sal pretreatment significantly improved left ventricular systolic function, as indicated by increased LVEF and LVFS, and reduced infarct size in I/R-injured rats, while effectively attenuating A/R-induced loss of H9c2 cell viability. The findings from the present study are consistent with previous reports demonstrating the cardioprotective and antioxidant properties of Sal in experimental models of myocardial injury (23,33,43,44). The present data further indicated that inhibition of oxidative stress-driven ferroptosis represents a critical mechanism by which Sal confers cardioprotection. Mechanistically, Sal interacted with the deubiquitinating enzyme USP11, increasing its thermal stability and its affinity for the antioxidant protein PRDX2, thereby promoting USP11-mediated deubiquitination and stabilization of PRDX2. Activation of this Sal-USP11-PRDX2 axis preserved intracellular redox homeostasis and prevented lethal lipid peroxidation, ultimately mitigating myocardial I/R injury (Fig. 7).

Accumulating evidence has established oxidative stress and ferroptosis as central pathological processes in myocardial I/R injury, particularly during the reperfusion phase (6,45,46). Ferroptosis is characterized by iron overload, GSH depletion, lipid peroxidation, downregulation of GPX4 and upregulation of PTGS2 (47), all of which were observed in the A/R and I/R models in the present study. In the present study, GPX4 and PTGS2 were assessed as downstream phenotypic indicators of ferroptosis and were not investigated as candidate direct substrates of USP11. PRDX2 functions as an important antioxidant protein by scavenging ROS and peroxides (29), and recent evidence has shown that USP11 can stabilize PRDX2 by reducing its ubiquitination (48). Loss of antioxidant capacity can promote ROS accumulation and lipid peroxidation, thereby favoring ferroptotic responses, in which GPX4 constitutes a major defense against lipid hydroperoxides and PTGS2 upregulation serves as a downstream phenotypic marker (49). In the present study, Sal treatment markedly reversed these ferroptotic features, exhibiting a protective profile comparable to that of the ferroptosis-specific inhibitor Fer-1. These findings strongly suggest that suppression of ferroptosis constitutes an essential component of Sal-mediated cardioprotection. Further mechanistic analyses revealed that USP11 expression was significantly reduced following A/R injury, whereas Sal restored USP11 levels. Molecular docking and CETSA assays supported an interaction between Sal and USP11, resulting in enhanced thermal stability of USP11. This interaction may have facilitated the association between USP11 and PRDX2 and promoted PRDX2 deubiquitination, thereby prolonging its protein half-life.

Due to the critical role of PRDX2 in scavenging excessive ROS and maintaining redox balance in cardiomyocytes (29,50), stabilization of PRDX2 effectively curtails lipid peroxidation and reduces susceptibility to ferroptotic cell death (51). A notable observation in the present study was that Sal treatment partially attenuated the accelerated degradation of PRDX2 even when USP11 was knocked down. This phenomenon is likely attributed to the inherent nature of transient siRNA transfection, which

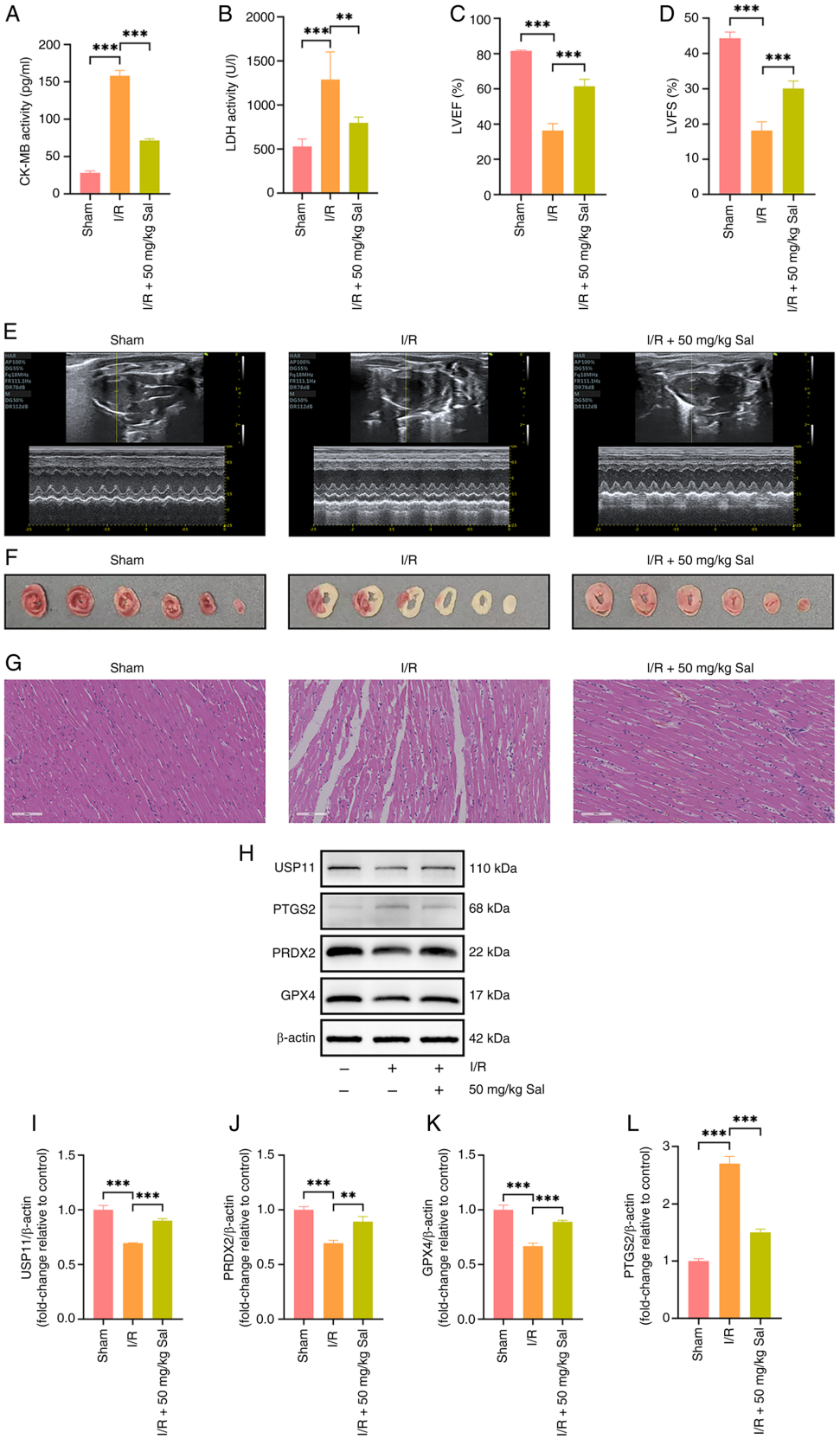

Figure 6. Sal pretreatment protects the myocardium against I/R injury. Serum levels of (A) CK-MB and (B) LDH were measured 2 h after reperfusion as markers of acute myocardial damage (n=6). (C) LVEF and (D) LVFS were quantified by echocardiography to evaluate cardiac contractile function (n=6). (E) Representative M-mode echocardiographic tracings (n=6). (F) Representative images of heart sections stained with 2% triphenyl tetrazolium chloride; white areas represent infarcted tissue, while red areas represent viable myocardium (n=3). (G) Representative H&E staining images (magnification, x400; scale bar, 400 μm) showing myocardial histopathological changes (n=3). (H) Representative immunoblot of USP11, PRDX2, GPX4 and PTGS2. Semi-quantitative analysis of (I) USP11, (J) PRDX2, (K) GPX4 and (L) PTGS2 in rat myocardial tissues (n=3). Data are presented as mean ± SD, with **P<0.01 and ***P<0.001 indicating statistical significance. Sal, salidroside; I/R, ischemia/reperfusion; CK-MB, creatine kinase isoenzyme; LDH, lactate dehydrogenase; LVEF, left ventricular ejection fraction; LVFS, left ventricular fractional shortening; USP11, ubiquitin-specific protease 11; PRDX2, peroxiredoxin 2; GPX4, glutathione peroxidase 4; PTGS2, prostaglandin-endoperoxide synthase 2.

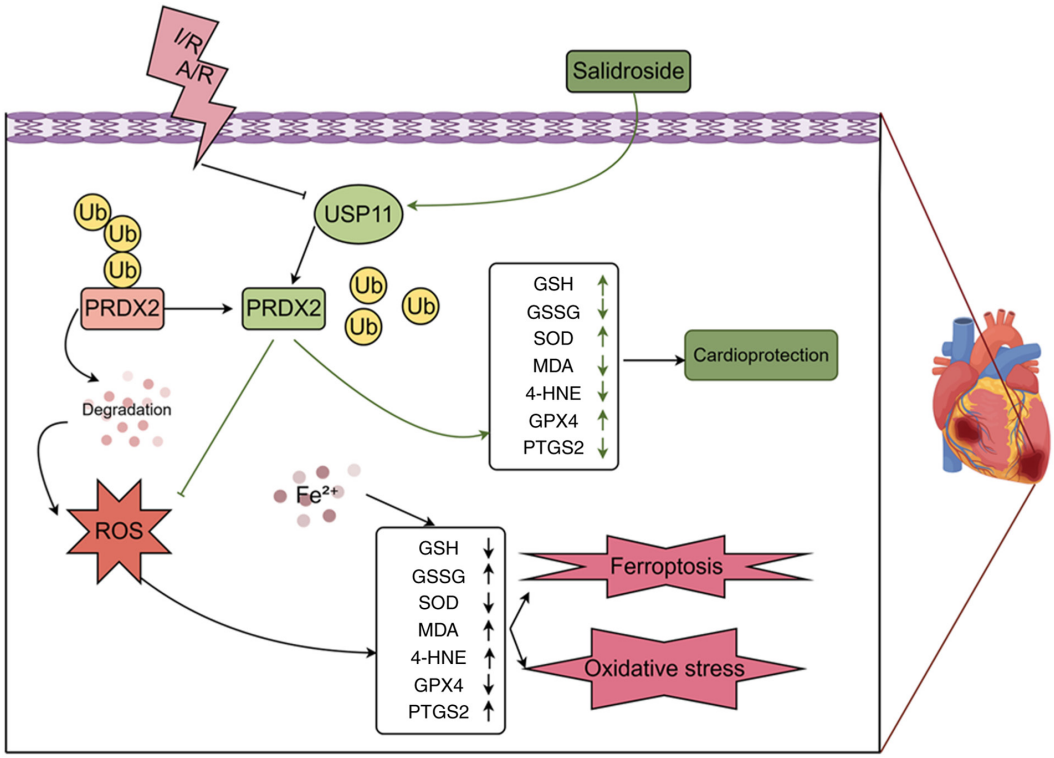

Figure 7. Schematic representation of the mechanism by which salidroside may attenuate myocardial I/R injury. I/R, ischemia/reperfusion; A/R, anoxia/reoxygenation; USP11, ubiquitin-specific protease 11; PRDX2, peroxiredoxin 2; ROS, reactive oxygen species; SOD, superoxide dismutase; MDA, malondialdehyde; GSH, glutathione; GSSG, glutathione disulfide; 4-HNE, 4-hydroxynonenal; GPX4, glutathione peroxidase 4; PTGS2, prostaglandin-endoperoxide synthase 2.

typically results in incomplete silencing of the target protein. Residual USP11 expression after incomplete siRNA-mediated knockdown may contribute to the partial restoration of PRDX2 stability by Sal. In addition, USP11-independent antioxidant mechanisms of Sal may also partially contribute to PRDX2 preservation. Compared with previous studies, the present work extends current understanding of the cardiovascular pharmacology of Sal by uncovering a novel post-translational regulatory mechanism. Earlier investigations have largely attributed the cardioprotective effects of Sal to activation of classical signaling pathways, such as PI3K/AKT, AMP-activated protein kinase or the nuclear factor erythroid 2-related factor 2/heme oxygenase-1 axis (52-54). While the present findings are generally consistent with the established antioxidant role of Sal, they further demonstrate that Sal exerts sustained cytoprotective effects by modulating protein stability through the ubiquitin-proteasome system.

In addition, the present study assigns a previously unrecognized role to USP11 in the context of cardiovascular disease. Although USP11 has been extensively studied in cancer biology and DNA damage repair (28,55,56), reports on its involvement in myocardial I/R injury and ferroptosis remain limited (57). Recent studies have implicated other deubiquitinating enzymes in ferroptosis regulation, including USP7 in $BRAF^{V600E}$-mutant thyroid cancer, where pharmacological inhibition of USP7 promotes ferroptosis, and BRCA1-associated protein 1 in inflammatory bowel disease, where it promotes ferroptosis through SLC7A11 suppression (58,59). The present data demonstrate that loss of USP11 accelerates PRDX2 degradation and increases ferroptotic vulnerability, identifying PRDX2 as a functional substrate of USP11 in H9c2 cells.

The present study proposes a 'small-molecule-deubiquitinase-antioxidant protein' regulatory paradigm, providing insight into how natural compounds exert cardioprotective effects by fine-tuning protein stability. Despite these encouraging findings, several limitations of the present study should be acknowledged. First, while direct C11-BODIPY lipid peroxidation staining and classical biochemical markers were examined to validate ferroptosis, future studies incorporating transmission electron microscopy to assess mitochondrial ultrastructure and testing a broader panel of targets (such as acyl-CoA synthetase long-chain family member 4 and solute carrier family 7 member 11) will provide a more exhaustive validation. Second, although the use of Fer-1 confirmed that ferroptosis is a critical component of myocardial A/R injury, it does not completely rule out the synergistic involvement of other cell death modalities, such as apoptosis or necrosis. Whether ferroptosis acts as the dominant form of cell death requires further broad-spectrum cross-validation using novel ferroptosis modulators such as Liproxstatin-1 or RAS-selective lethal small molecule 3. Third, while the CETSA and functional assays demonstrated that Sal may physically engage USP11 and promote USP11-dependent PRDX2 stabilization, the detailed upstream mechanisms, specifically whether Sal directly modulates USP11 transcription, baseline protein half-life or intrinsic catalytic activity, warrant further dedicated biochemical investigation. Additionally, while present data suggests target engagement, definitive validation of direct binding kinetics and the precise binding pocket will require future orthogonal biophysical assays (such as surface plasmon resonance) and targeted mutagenesis. Moreover, identifying the specific ubiquitin linkage type (such as K48

or K63) and employing catalytically inactive USP11 mutants or cell-free *in vitro* deubiquitination systems will be essential to fully elucidate the biochemical nuances of this interaction. Fourth, a pretreatment strategy was utilized to provide proof-of-concept for the prophylactic potential of Sal in anticipated I/R scenarios (such as scheduled coronary artery bypass grafting). Post-ischemic therapeutic administration remains to be evaluated for unpredictable acute events such as myocardial infarction. Fifth, while *in vitro* genetic silencing supported the functional involvement of USP11 in Sal-mediated protection, the *in vivo* rat model primarily demonstrated a robust phenotypic and molecular association. Definitive proof of *in vivo* causality will require future investigations employing adeno-associated virus-mediated cardiac-specific USP11 knockdown or knockout animal models. Sixth, the *in vivo* model relied on a single dose of Sal and lacked a Fer-1 positive control, limiting the characterization of dose-dependent pharmacological effects. Seventh, the *in vitro* mechanistic investigations were performed in the H9c2 cardiomyoblast cell line. While these findings were phenotypically supported by the *in vivo* adult rat model, future investigations employing primary rat cardiomyocytes will be essential to definitively validate this biochemical axis in mature cellular physiology.

In conclusion, the present study demonstrated that Sal attenuated myocardial I/R injury by promoting USP11-mediated deubiquitination and stabilization of PRDX2, thereby suppressing oxidative stress-induced ferroptosis.

Acknowledgements

Not applicable.

Funding

The present study was supported by the National Natural Science Foundation of China (grant nos. 82460057 and 82560074) and The First Affiliated Hospital of Nanchang University Young Talent Research Cultivation Fund (grant no. YFYPY202538).

Availability of data and materials

The data generated in the present study may be requested from the corresponding author.

Authors' contributions

ZCQ, JNL and YZL performed experiments, analyzed data and wrote the manuscript. ZMW and XDL performed experiments and analyzed data. RYZ and SQL analyzed and interpreted data. SQL, STZ and LW designed the experiments and provided financial support. SQL, STZ and LW confirm the authenticity of all the raw data. All authors have read and approved the final version of the manuscript.

Ethics approval and consent to participate

The present research protocol was reviewed and approved by the Ethics Committee of the First Affiliated Hospital of Nanchang University (approval no. CDYFY-IACUC-2025092003).

Patient consent for publication

Not applicable.

Competing interests

The authors declare that they have no competing interests.

References

1. Ferenczyová K, Kindernay L, Vlkovičová J, Kaločayová B, Rajtík T and Barteková M: Pharmacology of catechins in Ischemia-reperfusion injury of the heart. Antioxidants (Basel) 10: 1390, 2021.
2. Ghanta SN, Kattamuri LPV, Odueke A and Mehta JL: Molecular insights into Ischemia-reperfusion injury in coronary artery disease: Mechanisms and therapeutic implications: A comprehensive review. Antioxidants (Basel) 14: 213, 2025.
3. Francisco J and Del Re DP: Inflammation in myocardial Ischemia/reperfusion injury: Underlying mechanisms and therapeutic potential. Antioxidants (Basel) 12: 1944, 2023.
4. Zhang J, Zhao Y and Gong N: Endoplasmic reticulum stress signaling modulates ischemia/reperfusion injury in the aged heart by regulating mitochondrial maintenance. Mol Med 30: 107, 2024.
5. Davidson SM, Ferdinandy P, Andreadou I, Bøtker HE, Heusch G, Ibáñez B, Ovize M, Schulz R, Yellon DM, Hausenloy DJ, *et al*: Multitarget strategies to reduce myocardial Ischemia/Reperfusion injury: JACC review topic of the week. J Am Coll Cardiol 73: 89-99, 2019.
6. Zhang T, Deng W, Deng Y, Liu Y, Xiao S, Luo Y, Xiang W and He Q: Mechanisms of ferroptosis regulating oxidative stress and energy metabolism in myocardial ischemia-reperfusion injury and a novel perspective of natural plant active ingredients for its treatment. Biomed Pharmacother 165: 114706, 2023.
7. Fang X, Ardehali H, Min J and Wang F: The molecular and metabolic landscape of iron and ferroptosis in cardiovascular disease. Nat Rev Cardio 20: 7-23, 2023.
8. Chen X, Kang R, Kroemer G and Tang D: Broadening horizons: The role of ferroptosis in cancer. Nat Rev Clin Oncol 18: 280-296, 2021.
9. Yan HF, Zou T, Tuo QZ, Xu S, Li H, Belaidi AA and Lei P: Ferroptosis: Mechanisms and links with diseases. Signal Transduct Target Ther 6: 49, 2021.
10. Galaris D, Barbouti A and Pantopoulos K: Iron homeostasis and oxidative stress: An intimate relationship. Biochim Biophys Acta Mol Cell Res 1866: 118535, 2019.
11. Yu Y, Yan Y, Niu F, Wang Y, Chen X, Su G, Liu Y, Zhao X, Qian L, Liu P and Xiong Y: Ferroptosis: A cell death connecting oxidative stress, inflammation and cardiovascular diseases. Cell Death Discov 7: 193, 2021.
12. Tang D, Chen X, Kang R and Kroemer G: Ferroptosis: Molecular mechanisms and health implications. Cell Res 31: 107-125, 2021.
13. Stockwell BR: Ferroptosis turns 10: Emerging mechanisms, physiological functions, and therapeutic applications. Cell 185: 2401-2421, 2022.
14. Liu J, Kuang F, Kroemer G, Klionsky DJ, Kang R and Tang D: Autophagy-dependent ferroptosis: Machinery and regulation. Cell Chem Biol 27: 420-435, 2020.
15. Sun S, Wu Y, Maimaitijiang A, Huang Q and Chen Q: Ferroptotic cardiomyocyte-derived exosomes promote cardiac macrophage M1 polarization during myocardial infarction. PeerJ 10: e13717, 2022.
16. Xu C, Liu Y, Yang J, Zhai M, Fan Z, Qiao R, Jin P and Yang L: Effects of berbamine against myocardial ischemia/reperfusion injury: Activation of the 5'adenosine monophosphate-activated protein kinase/nuclear factor erythroid 2-related factor pathway and changes in the mitochondrial state. Biofactors 48: 651-664, 2022.
17. Peoples JN, Saraf A, Ghazal N, Pham TT and Kwong JQ: Mitochondrial dysfunction and oxidative stress in heart disease. Exp Mol Med 51: 1-13, 2019.
18. Remex NS, Abdullah CS, Aishwarya R, Sinha MH, Dhar P, Dhaou CB, Orr AW and Bhuiyan MS: Deletion of Sigmar1 leads to increased arterial stiffness and altered mitochondrial respiration resulting in vascular dysfunction. Front Cardiovasc Med 15: 1386296, 2024.

19. Matsushima S and Sadoshima J: Yin and yang of NADPH oxidases in myocardial Ischemia-reperfusion. Antioxidants (Basel) 11: 1069, 2022.
20. Li HX, Wang TH, Wu LX, Xue FS, Zhang GH and Yan T: Role of Keap1-Nrf2/ARE signal transduction pathway in protection of dexmedetomidine preconditioning against myocardial ischemia/reperfusion injury. Biosci Rep 42: BSR20221306, 2022.
21. Zheng Y, Mao L, Wang Q, Hu H, Xarpidin B, Luo Z and Wu YL: Mitochondria-targeted ROS scavenging natural enzyme cascade nanogels for periodontitis treatment via hypoxia alleviation and immunomodulation. Adv Sci (Weinh) 12: e07481, 2025.
22. Dodson M, Castro-Portuguez R and Zhang DD: NRF2 plays a critical role in mitigating lipid peroxidation and ferroptosis. Redox Biol 23: 101107, 2019.
23. Zhang X, Xie L, Long J, Xie Q, Zheng Y, Liu K and Li X: Salidroside: A review of its recent advances in synthetic pathways and pharmacological properties. Chem Biol Interact 339: 109268, 2021.
24. Chang X, Zhang K, Zhou R, Luo F, Zhu L, Gao J, He H, Wei T, Yan T and Ma C: Cardioprotective effects of salidroside on myocardial ischemia-reperfusion injury in coronary artery occlusion-induced rats and Langendorff-perfused rat hearts. Int J Cardiol 215: 532-544, 2016.
25. Sun YM, Wang XY, Zhou XR, Zhang C, Liu KJ, Zhang FY and Xiang B: Salidroside Ameliorates radiation damage by reducing mitochondrial oxidative stress in the submandibular gland. Antioxidants (Basel) 11: 1414, 2022.
26. Zhang Y, Hailati J, Ma X, Midilibieke H and Liu Z: Ubiquitin-specific protease 11 Aggravates Ischemia-reperfusion-induced Cardiomyocyte Pyroptosis and injury by promoting TRAF3 Deubiquitination. Balkan Med J 40: 205-214, 2023.
27. Rajkumar S, Jung JH, Kim JY, Karapurkar JK, Birappa G, Gowda DAA, Ajaykumar CB, Perumalsamy H, Suresh B, Kim KS, *et al*: Loss of Ubiquitin-specific protease 11 mitigates pulmonary fibrosis in human pluripotent stem Cell-derived alveolar organoids. Int J Stem Cells 18: 205-213, 2025.
28. Zhu J, Sun R, Sun K, Yan C, Jiang J, Kong F and Shi J: The deubiquitinase USP11 ameliorates intervertebral disc degeneration by regulating oxidative stress-induced ferroptosis via deubiquitinating and stabilizing Sirt3. Redox Biol 62: 102707, 2023.
29. Balasubramanian P, Vijayarangam V, Deviparasakthi MKG, Palaniyandi T, Ravi M, Natarajan S, Viswanathan S, Baskar G, Wahab MRA and Surendran H: Implications and progression of peroxiredoxin 2 (PRDX2) in various human diseases. Pathol Res 254: 155080, 2024.
30. Han F, Dong Y, Liu Q, Song L, Guo H, Zhu L, Sun B, Zhao W and Chen L: S-nitrosylation of peroxiredoxin 2 exacerbates hyperuricemia-induced renal injury through regulation of mitochondrial homeostasis. Free Radic Biol Med 230: 66-78, 2025.
31. Zhang Y, Sun C, Xiao G, Shan H, Tang L, Yi Y, Yu W and Gu Y: S-nitrosylation of the Peroxiredoxin-2 promotes S-nitrosoglutathione-mediated lung cancer cells apoptosis via AMPK-SIRT1 pathway. Cell Death Dis 10: 329, 2019.
32. Zhao ST, Qiu ZC, Xu ZQ, Tao ED, Qiu RB, Peng HZ, Zhou LF, Zeng RY, Lai SQ and Wan L: Curcumin attenuates myocardial ischemia-reperfusion-induced autophagy-dependent ferroptosis via Sirt1/AKT/FoxO3a signaling. Int J Mol Med 55: 51, 2025.
33. Yang B, Xu Y, Yu J, Wang Q, Fan Q, Zhao X, Qiao Y, Zhang Z, Zhou Q, Yin D, *et al*: Salidroside pretreatment alleviates ferroptosis induced by myocardial ischemia/reperfusion through mitochondrial superoxide-dependent AMPKα2 activation. Phytomedicine 128: 155365, 2024.
34. American Veterinary Medical Association: AVMA guidelines for the euthanasia of animals. 2020 Edition. American Veterinary Medical Association; Schaumburg, IL, 2020.
35. Zhao ST, Qiu ZC, Zeng RY, Zou HX, Qiu RB, Peng HZ, Zhou LF, Xu ZQ, Lai SQ and Wan L: Exploring the molecular biology of ischemic cardiomyopathy based on ferroptosis-related genes. Exp Ther Med 27: 221, 2024.
36. Martinez Molina D, Jafari R, Ignatushchenko M, Seki T, Larsson EA, Dan C, Sreekumar L, Cao Y and Nordlund P: Monitoring drug target engagement in cells and tissues using the cellular thermal shift assay. Science 341: 84-87, 2013.
37. Jafari R, Almqvist H, Axelsson H, Ignatushchenko M, Lundbäck T, Nordlund P and Martinez Molina D: The cellular thermal shift assay for evaluating drug target interactions in cells. Nat Protoc 9: 2100-2122, 2014.
38. Savitski MM, Reinhard FB, Franken H, Werner T, Savitski MF, Eberhard D, Martinez Molina D, Jafari R, Dovega RB, Klaeger S, *et al*: Tracking cancer drugs in living cells by thermal profiling of the proteome. Science 346: 1255784, 2014.
39. Huang J, Yang Q, Zeng L and Deng K: Multi-omics network toxicology reveals the role of benzo[a]pyrene in ovarian cancer: Integrating gut microbiota dynamics and Mendelian randomization. Ecotoxicol Environ Saf 302: 118601, 2025.
40. Liu Y, Yang X, Gan J, Chen S, Xiao ZX and Cao Y: CB-Dock2: Improved protein-ligand blind docking by integrating cavity detection, docking and homologous template fitting. Nucleic Acids Res 50: W159-W164, 2022.
41. Harper S, Gratton HE, Cornaciu I, Oberer M, Scott DJ, Emsley J and Dreveny I: Structure and catalytic regulatory function of ubiquitin specific protease 11 N-terminal and ubiquitin-like domains. Biochemistry 53: 2966-2978, 2014.
42. Wang X, Wang Z, Cao J, Dong Y and Chen Y: Melatonin alleviates acute sleep Deprivation-Induced memory loss in mice by suppressing hippocampal ferroptosis. Front Pharmacol 12: 708645, 2021.
43. Feng T, Shi J, Zhao J, Zhao Q, Wang T, Wan S, Fan C, Wang S, Lai C and Yao Y: Salidroside can protect against ferroptosis in cardiomyocytes and may be related to the regulation of GGT1. Front Pharmacol 16: 1580506, 2025.
44. Tian X, Huang Y, Zhang X, Fang R, Feng Y, Zhang W, Li L and Li T: Salidroside attenuates myocardial ischemia/reperfusion injury via AMPK-induced suppression of endoplasmic reticulum stress and mitochondrial fission. Toxicol Appl Pharmacol 448: 116093, 2022.
45. He J, Liu D, Zhao L, Zhou D, Rong J, Zhang L and Xia Z: Myocardial ischemia/reperfusion injury: Mechanisms of injury and implications for management (Review). Exp Ther Med 23: 430, 2022.
46. Li JY, Liu SQ, Yao RQ, Tian YP and Yao YM: A novel insight into the fate of cardiomyocytes in Ischemia-reperfusion injury: From iron metabolism to ferroptosis. Front Cell Dev Biol 9: 799499, 2021.
47. Du YW, Li XK, Wang TT, Zhou L, Li HR, Feng L, Ma H and Liu HB: Cyanidin-3-glucoside inhibits ferroptosis in renal tubular cells after ischemia/reperfusion injury via the AMPK pathway. Mol Med 29: 42, 2023.
48. Kong F, Luan J, Pan Q, Qiao Y and Wang W: Ubiquitination-mediated PRDX2 alleviates intervertebral disc degeneration via restraining TBHP-induced nucleus pulposus cell apoptosis, ferroptosis and ECM degradation. J Inflamm (Lond) 23: 15, 2026.
49. Yang WS, SriRamaratnam R, Welsch ME, Shimada K, Skouta R, Viswanathan VS, Cheah JH, Clemons PA, Shamji AF, Clish CB, *et al*: Regulation of ferroptotic cancer cell death by GPX4. Cell 156: 317-331, 2014.
50. Zhang H, Xu T, Mei X, Zhao Q, Yang Q, Zeng X, Ma Z, Zhou H, Zeng Q, Xu D and Ren H: PINK1 modulates Prdx2 to reduce lipotoxicity-induced apoptosis and attenuate cardiac dysfunction in heart failure mice with a preserved ejection fraction. Clin Transl Med 15: e70166, 2025.
51. Li H, Yang H, Wang D, Zhang L and Ma T: Peroxiredoxin2 (Prdx2) reduces oxidative stress and apoptosis of myocardial cells induced by acute myocardial infarction by inhibiting the TLR4/Nuclear factor kappa B (NF-κB) signaling pathway. Med Sci Monit 26: e926281, 2020.
52. Liu Q, Luo Q, Zhong B, Tang K, Chen X, Yang S and Li X: Salidroside attenuates myocardial remodeling in DOCA-salt-induced mice by inhibiting the endothelin 1 and PI3K/AKT/NFκB signaling pathways. Eur J Pharmacol 962: 176236, 2024.
53. Zhang L, Liu Y, Hua Z, Qin Y, Wang T, Li N and Song L: Salidroside alleviates cardiomyocyte senescence by activating the AMPK-mediated signaling pathway. J Mol Histol 56: 252, 2025.
54. Wang N, Zuo Z, Meng T, Liu Y, Zheng X and Ma Y: Salidroside alleviates simulated microgravity-induced bone loss by activating the Nrf2/HO-1 pathway. J Orthop Surg Res 19: 531, 2024.
55. Ting X, Xia L, Yang J, He L, Si W, Shang Y and Sun L: USP11 acts as a histone deubiquitinase functioning in chromatin reorganization during DNA repair. Nucleic Acids Res 47: 9721-9740, 2019.
56. Zhu X, Zhang Y, Luo Q, Wu X, Huang F, Shu T, Wan Y, Chen H and Liu Z: The deubiquitinase USP11 promotes ovarian cancer chemoresistance by stabilizing BIP. Signal Transduct Target Ther 6: 264, 2021.

57. Liao Y, Zhou D, Wang P, Yang M and Jiang N: Ubiquitin specific peptidase 11 as a novel therapeutic target for cancer management. Cell Death Discov 8: 292, 2022.
58. Hu C, Tian W, Tang Y, Wang P, Kuan T, Wei W, Chen D, Li P and Su X: USP7 inhibitor P5091 enhances the antitumor efficacy of vemurafenib in BRAFV600E-mutant thyroid cancer via ferroptosis. Biochem Pharmacol 243: 117522, 2026.
59. Chen X, Yang Y, Han B, Zhou Z, Xu C, Gu M, Huang Z, Liu H, Ren K and Luan Y: BAP1 exacerbates inflammatory bowel disease by promoting ferroptosis via SLC7A11 suppression. Int Immunopharmacol 160: 114957, 2025.